The Influence of Lithium Vacancy Defects on Tritium Diffusion in $\beta-Li_2TiO_3$

Kamal N. Goswami[,†] and Samuel T. Murphy[*,,†]

E-mail: samuel.murphy@lancaster.ac.uk

Phone: +44 (0)1524 592671

Abstract

Lithium metatitianate, Li_2TiO_3, is a leading candidate for application as a tritium breeding material in a future fusion reactor. Following transmutation of lithium, the tritium must escape the crystal in order to be extracted for use in the fusion plasma. The rate limiting step to tritium release from the Li_2TiO_3 pebbles is diffusion through the crystal grains. In this work, the activation barriers for tritium diffusion have been calculated using density functional theory (DFT). The results show that tritium can diffuse as an interstitial with a barrier of 0.52 eV. However, when a tritium ion becomes bound to a lithium vacancy defect, the energy required for either the tritium to detrap from the vacancy or for the cluster to diffuse increase to >1 eV. Overall, these results suggest that the introduction of lithium vacancies due to Li burn-up may lead to an increase in tritium retention in the pebbles.

Introduction

Future fusion reactors will employ the reaction between deuterium and tritium to release energy for electricity generation. Since there is very limited naturally occurring tritium, it is expedient to generate it *in-situ* from the transmutation of lithium using the high energy

neutron ejected from the D-T reaction. This will be done by surrounding the plasma chamber with a blanket region containing a lithium breeder material. A number of different blanket concepts have been proposed, mostly based on either lithium ceramic pebbles or a liquid lithium lead eutectic.[1]

To ensure that the fusion process is sustainable it is essential that at least one tritium is recovered from the blanket for each fusion reaction in the plasma. Due to the inability to completely surround the plasma with blanket and the permeation of tritium into other reactor components, a tritium breeding ratio (TBR) greater than 1.1 is necessary.[2] In the case of a solid breeder, the high energy neutrons will penetrate the pebbles leading to tritium being generated throughout the ceramic matrix. Therefore, it is essential that all tritium generated can be extracted from the breeder material to ensure the maximum possible TBR. For recovery this tritium must diffuse to the surface as illustrated in Figure 1. Following transmutation, the tritium must be accommodated in the ceramic's microstructure, before diffusing through the crystal grains until it reaches the grain boundary. It will then diffuse along the boundary until reaching the pebble surface. Once at the surface, tritium will undergo isotope exchange reactions with hydrogen in the He purge gas before being recovered.

The rate limiting step to tritium recovery is diffusion in the fuel grains. Multiple peaks in thermal desorption spectra of neutron irradiated lithium ceramics, show that there are a number of distinct mechanisms contributing to the tritium release process, with their relative importance depending on temperature.[3,4] Previous studies have used these experimental observations to infer the specific release mechanisms and what defects are facilitating them, however, there is no consensus on what these may be. Experimental activation energies for tritium diffusion vary from 0.63-1.5 eV for Li_2TiO_3 [5–7] . The experimental data shows a significant variation that is likely due to the different experimental conditions, including burn-ups, and does not allow the isolation of the individual mechanism for tritium diffusion and their associated energy.

Previous atomistic simulations have shown that the mode of tritium accommodation in

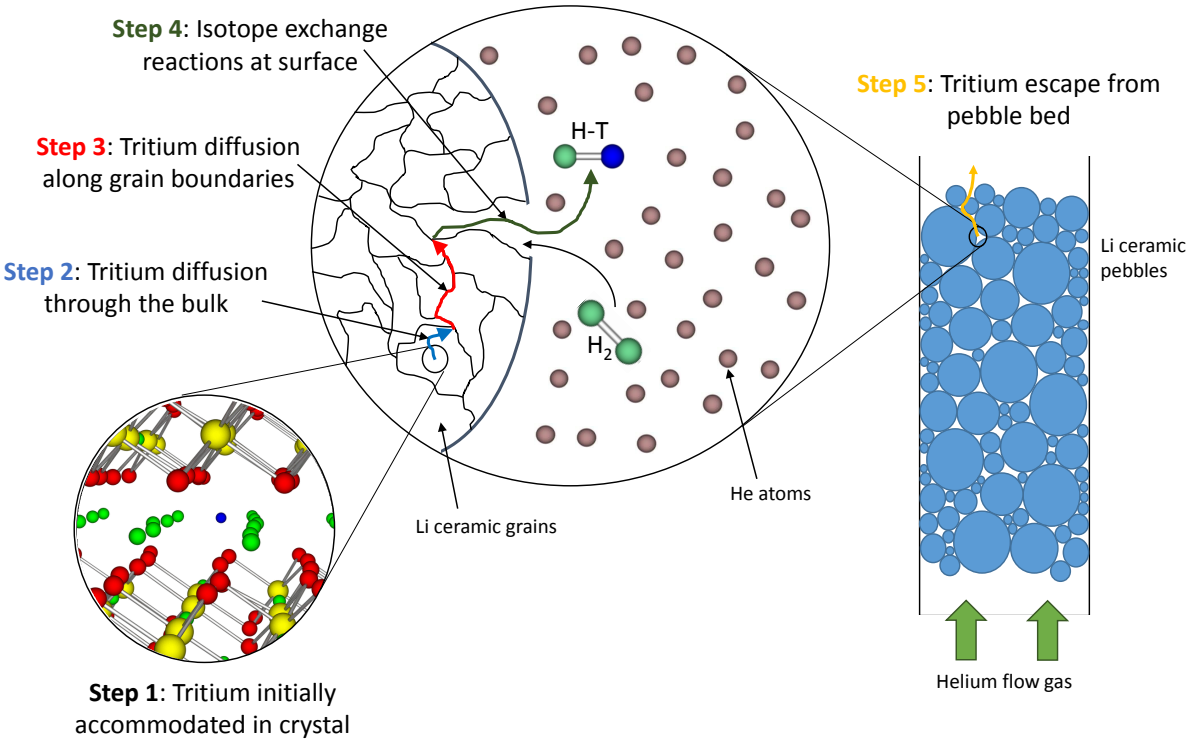

Figure 1: Schematic of the tritium release process from lithium ceramic pebbles in breeder blanket

Li_2TiO_3 depends on the stoichiometry of the underlying crystal.[8] Under conditions where there is a lithium excess, the tritium is predicted to sit as an interstitial that bonds to an oxygen ion, forming a hydroxyl group. The excess positive charge is then compensated by a variety of different mechanisms, depending on the conditions. Under conditions of lithium deficiency, such as those anticipated as the ceramic ages, these hydroxyl groups become bound to lithium vacancy defects forming the $\{T_i^{+1} : V_{Li}^{-1}\}^0$ complex.[8]

As the availability of point defects changes, so too does the tritium diffusion mechanism. Shi *et al.* used density functional theory (DFT) to examine the diffusion of charged tritium interstitials in Li_2TiO_3.[9] They observed that the activation energy for diffusion in the *xy*-plane is 0.33 eV, while for tritium to migrate in the z direction the barrier is much higher at 1.00 eV. This high degree of anisotropy in the tritium mobility arises due to the complex layered structure exhibited by Li_2TiO_3. Li *et al.* have also employed DFT to study tritium diffusion in Li_2TiO_3 in the presence of lithium vacancy defects and determined that the energy barrier for a tritium to escape from the $\{T_i^{+1} : V_{Li}^{-1}\}^0$ complex is 0.76 eV.[10] This result implies that as the fuel ages and lithium is burnt up the activation energy for tritium release will increase. However, these works have neglected the mobility of the lithium vacancy itself and the possibility that the lithium vacancy may assist tritium diffusion through a co-operative mechanism. Therefore, the aim of the present work is to re-examine the complex tritium diffusion mechanisms in Li_2TiO_3 considering the role of the lithium vacancy.

Crystallography

The β-phase of Li_2TiO_3 is stable across a wide temperature range of 300° C to 1215°C, as is seen from the Li_2O-TiO_2 phase diagram,[11,12] while the cubic α and γ-phases are present at temperatures above and below this range respectively. The structure of β-Li_2TiO_3 was first studied by Lang[13] and later refined by Kataoka *et al.*[14] using X-ray diffraction of large single crystals. These works described Li_2TiO_3 as a distorted rocksalt structure with alternating

(111) planes of Li_6, O_6, Li_2Ti_4 and O_6. In the mixed cation layer of Li_2Ti_4, six Ti ions surround a Li ion forming a hexagon. At low sintering temperatures a number of different stacking sequences, corresponding to different space groups, *viz.* C2/m, C2/c and $P3_112$, are observed.[15] However, in the present work, it is assumed that sintering took place at high temperature and so only the monoclinic C2/c space group is present. An illustration of β-Li_2TiO_3 is presented in Figure 2. The experimental lattice parameters of β-Li_2TiO_3 according to Kataoka *et al.* are $a = 5.0623$ Å, $b = 8.7876$ Å, $c = 9.7533$ Å and $\beta = 100.212°$.[14]

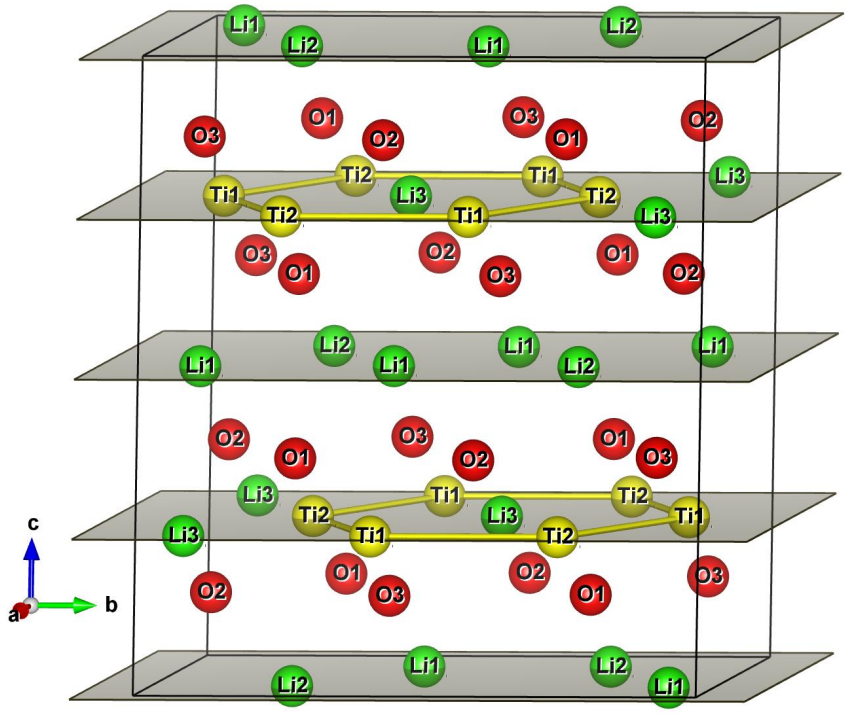

Figure 2: Unit cell of $\beta-Li_2TiO_3$ showing the different ions and their types. The Li, Ti and O ions are shown as green, yellow and red spheres respectively. The Li_6 and Li_2Ti_4 layers have been highlighted, and the O ions lie above or below these layers. Also illustrated are the Ti-Ti bonds in the Li_2Ti_4 layers with a Li ion in the centre to illustrate the hexagonal structure.

As shown in Figure 2, there are three symmetrically distinct lithium lattice sites in β-Li_2TiO_3. Li1 and Li2 are found in the pure lithium layer, while Li3 is found at the centre of the Ti hexagons in the mixed cation layer. Therefore, the different positions have different

nearest neighbour cation environments, as illustrated in Figure 3. In fact, the Li1 and Li2 positions are remarkably similar and have almost identical vacancy formation energies.[16] In the pure lithium layer, a Li1 ion is surrounded by an equal number of Li1 and Li2 ions. By contrast a Li2 ion is surrounded by Li1 ions only. Due to the relative location of Ti ions above and below the xy-planes for Ti-Ti and Li-Li bond distances are distorted.

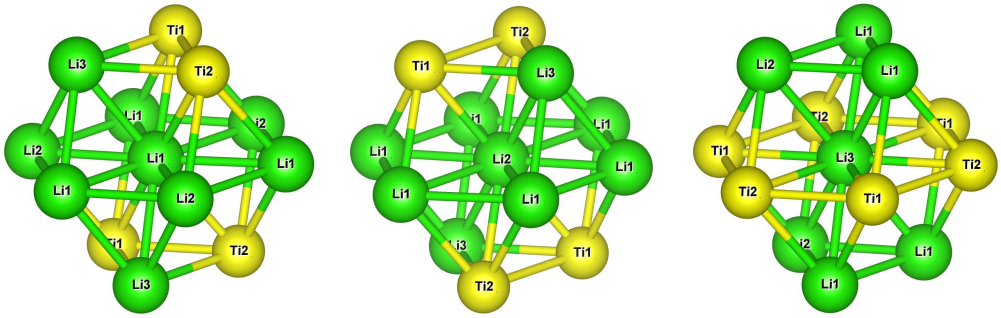

(a) Li1 (b) Li2 (c) Li3

Figure 3: Local environments surrounding the lithium sites in Li_2TiO_3. Note that the oxygen ions have been removed to highlight the cation environments around the different lithium sites.

As β-Li_2TiO_3 exhibits a distorted rocksalt structure, the lithium ions are octahedrally co-ordinated with oxygen as illustrated in Figure 4. These oxygen ions have been designated A - F as illustrated in Figure 4.

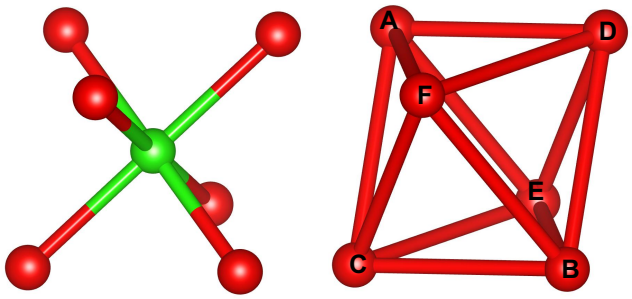

(a) (b)

Figure 4: (a) The Li ion is coordinated by six oxygen ions (b) The octahedron formed by the oxygen ions designated A - F around the Li vacancy.

Computational Details

All first principles calculations in the present work were based on Density Functional Theory[17,18] and were performed using the planewave CASTEP simulation package.[19,20] The Generalized Gradient Approximation (GGA) parameterised by Perdew, Burke and Ernzerhof (PBE) was used as exchange-correlation functional.[21] All calculations were performed using a supercell containing $2 \times 1 \times 1$ replications of the unitcell for a total of 96 atoms. This relatively small simulation supercell may be susceptible to finite size effects due to the interaction of the charged defects with their periodic images.[22] However, these finite-size effects cancel for the calculation of migration barriers. Ultrasoft pseudopotentials were employed with a planewave cutoff energy cutoff of 600 eV. A Monkhorst-Pack scheme[23] was used to sample the Brillouin zone with a density of 0.06 Å^{-1} which corresponded to a $2 \times 2 \times 2$ k-point mesh in the $2 \times 1 \times 1$ supercell. A Methfessel-Paxton smearing width of 0.1 eV was used.[24] To test the efficacy of the model an energy minimisation of the perfect unitcell was performed and the lattice parameters obtained were $a = 5.1186$ Å, $b = 8.8809$ Å, $c = 9.8976$ Å and $\beta = 100.212°$ in good agreement with the experimental values of Kataoka *et al.*[14]

Transition states were determined by performing an energy minimisation of the start and end structures under constant volume conditions until all forces fell below 0.08 eV/Å. Activation energies were calculated using the complete Linear/Quadratic Synchronous Transit (LST/QST)[25] method with default settings as implemented in CASTEP. Note that more stringent conditions were tested and this did not significantly affect the results.

A complete understanding of the tritium release process from ceramic materials such as Li_2TiO_3 requires an examination of all the possible atomic scale hops that may contribute to the diffusion process. As discussed in the introduction, this is not solely dependent on the migration barriers for tritium hops themselves, but also other defects that may promote or hinder tritium diffusion. Previous studies have indicated that the lithium vacancy defect will play an important role in the tritium release process as the material ages. Therefore, this study will examine the migration barriers for diffusion of the isolated lithium vacancy

and tritium interstitial defects as well as the barriers to diffusion of the bound $\{T_i^{+1} : V_{Li}^{-1}\}^0$ cluster.

The interstitial sites between the Li and O layers were initially located by performing geometry optimization calculations with a tritium ion (T^{+1}) initially placed in the vicinity of the oxygen ions. Once the locations of the initial and final positions of the ions were identified the LST/QST method was used to calculate the energy barrier between them. A similar approach was used to locate the tritium interstitial sites within the lithium vacancies. In this case the positions were located by performing geometry optimization calculations of tritium ions initially positioned halfway between the vacancy and the oxygen ions.

Results and Discussion

Lithium Vacancy Diffusion

In the first instance the activation energies for diffusion of the lithium vacancy, V_{Li}^{1-}, defects in Li_2TiO_3 were determined. Within the C2/c space group there are three types of lithium site. Two of these are in the pure lithium layer and the third is at the centre of the Ti hexagons in the mixed cation layer as illustrated in Figure 3. While there are only three symmetrically distinct lithium sites present in Li_2TiO_3, the arrangement of these sites is such that there are a number of different possible hops between them, as discussed by Kuganathan *et al.*[26] For completeness barriers for all possible pathways between nearest neighbour lithium sites were calculated. The resulting barriers for Li1 and Li2 vacancy diffusion are presented in Table 1 and that for Li3 vacancy diffusion are presented in Table 2.

The calculated activation energies are between 0.41 and 0.67 eV, which is in the range of energies predicted by experiment.[27–29] The lowest energy barriers correspond to the vacancy hopping from the pure Li layer into the mixed cation layer, with the hop from the Li2 site being very slightly lower in energy than from the Li1 site (0.41 eV compared to 0.45 eV). The ordering of the hops between the pure lithium and mixed cation layer is in excellent

Table 1: Calculated intrinsic Li1 and Li2 vacancy diffusion barriers for the nearest-neighbour (NN) hops as shown in Figure 3, assuming the vacancy occupies the central ionic position. The distances, d, presented in the table were calculated in the perfect crystal of Kataoka *et al.*[14] There are six possible hops in the same xy-plane and one each above and below the xy-plane.

Class	Pathway	d (Å)	Barrier (eV)		Pathway	d (Å)	Barrier (eV)	
			Forward	Reverse			Forward	Reverse
xy-plane above	$V_{Li1}^{1-} \rightarrow V_{Li3}^{1-}$	2.91	0.45	0.51	$V_{Li2}^{1-} \rightarrow V_{Li3}^{1-}$	2.92	0.41	0.47
same xy-plane	$V_{Li1}^{1-} \rightarrow V_{Li1}^{1-}$	3.00	0.65	0.65	$V_{Li2}^{1-} \rightarrow V_{Li1}^{1-}$	2.99	0.67	0.67
	$V_{Li1}^{1-} \rightarrow V_{Li1}^{1-}$	2.79	0.50	0.50	$V_{Li2}^{1-} \rightarrow V_{Li1}^{1-}$	2.99	0.67	0.67
	$V_{Li1}^{1-} \rightarrow V_{Li1}^{1-}$	3.00	0.65	0.65	$V_{Li2}^{1-} \rightarrow V_{Li1}^{1-}$	2.90	0.57	0.57
	$V_{Li1}^{1-} \rightarrow V_{Li2}^{1-}$	2.89	0.55	0.54	$V_{Li2}^{1-} \rightarrow V_{Li1}^{1-}$	2.90	0.57	0.57
	$V_{Li1}^{1-} \rightarrow V_{Li2}^{1-}$	2.90	0.57	0.57	$V_{Li2}^{1-} \rightarrow V_{Li1}^{1-}$	2.89	0.54	0.55
	$V_{Li1}^{1-} \rightarrow V_{Li2}^{1-}$	2.99	0.67	0.67	$V_{Li2}^{1-} \rightarrow V_{Li1}^{1-}$	2.89	0.54	0.55
xy-plane below	$V_{Li1}^{1-} \rightarrow V_{Li3}^{1-}$	2.91	0.45	0.51	$V_{Li2}^{1-} \rightarrow V_{Li3}^{1-}$	2.92	0.41	0.47

Table 2: Calculated intrinsic Li3 vacancy diffusion barriers for the nearest-neighbour (NN) hops as shown in Figure 3, assuming the vacancy occupies the central ionic position. The distances presented in the table were calculated from the perfect crystal of Kataoka *et al.*[14] There were three possible hops each in the *xy*-planes above and below the *xy*-plane.

Class	Pathway	d (Å)	Barrier (eV)	
			Forward	Reverse
xy-plane above	$V_{Li3}^{1-} \rightarrow V_{Li1}^{1-}$	2.91	0.51	0.45
	$V_{Li3}^{1-} \rightarrow V_{Li1}^{1-}$	2.91	0.51	0.45
	$V_{Li3}^{1-} \rightarrow V_{Li2}^{1-}$	2.92	0.47	0.41
xy-plane below	$V_{Li3}^{1-} \rightarrow V_{Li1}^{1-}$	2.91	0.51	0.45
	$V_{Li3}^{1-} \rightarrow V_{Li1}^{1-}$	2.91	0.51	0.45
	$V_{Li3}^{1-} \rightarrow V_{Li2}^{1-}$	2.92	0.47	0.41

agreement with the previous DFT simulations of Islam and Bredow.[30] In this previous work there was only one transition within the pure lithium considered which had an energy of 0.45 eV for the forward process and for the reverse process an energy of 0.5 eV was determined. These values are slightly lower than those predicted here which are all in the range 0.5-0.67 eV. It should be noted that this previous work examined charge neutral vacancies while here the fully charged V_{Li}^{1-} defects are considered and this may account for the small discrepancy. Mukai *et al.* calculated barriers of 0.52 eV and 0.53 eV for the $V_{Li3}^{-1} \rightarrow V_{Li1}^{-1}$ and $V_{Li2}^{-1} \rightarrow V_{Li1}^{-1}$ hops.[29] These values are in excellent agreement with the values of 0.51 eV and 0.54 eV calculated here. However, for the $V_{Li2}^{-1} \rightarrow V_{Li1}^{-1}$ hops, two additional values of 0.57 eV and 0.67 eV were also calculated. Kuganathan *et al.* predict that the lowest energy process is for vacancy migration in the pure Li layer with a barrier of 0.39 eV, while the energy to transfer between the two layers is much higher at 0.65 and 0.67 eV.[26] Further barriers for migration of a lithium vacancy were determined by Vijayakumar *et al.* who found values in the range 0.2-0.3 eV.[31] These last two studies employed empirical pair potentials that are not able to consider charge transfer during the migration process and are, therefore, likely to be less reliable than the DFT data presented here.

Overall, the data suggests that there is a slight anisotropy in the vacancy mediated diffusion of lithium in Li_2TiO_3 with diffusion in the z-direction having slightly lower energy barriers than diffusion in the xy-plane.

Tritium Diffusion

Tritium Diffusion as an Interstitial

This next section considers tritium diffusing as an interstitial defect. As discussed by Shi *et al.* there are six symmetrically distinct tritium interstitial sites in Li_2TiO_3.[9] These positions are illustrated in Figures 5 and 6 and the fractional co-ordinates are presented in Table 3. In all cases the tritium ions are bonded to oxygen ions in the form of hydroxyl groups as observed in previous work.[8]

Table 3: Calculated fractional coordinates of the different types of interstitial sites for tritium in β-Li_2TiO_3

Position	Site Label	Fractional Coordinates (x,y,z)	Host Oxygen
Li_6 layer	1	0.21310, 0.08659, 0.46836	O2
	2	0.44976, 0.26219, 0.46833	O1
	3	0.20159, 0.40395, 0.47633	O3
O_6 layer	4	0.36446, 0.58707, 0.40740	O2
	5	0.26578, 0.32535, 0.59409	O1
	6	0.23561, 0.50323, 0.39167	O3

The calculated activation energies and jump distances for the hops between different tritium interstitial positions are presented in Table 4, where they are compared to the values of Shi *et al.*[9] For simplicity, the possible diffusion processes are grouped into three distinct classes, C1, C2 and C3. The first class, C1, involves tritium hopping within the layer of interstitial positions closest to the Li_6 layer encompassing the 1, 2 and 3 tritium sites (see Figures 5 and 6). The second, C2, class corresponds to the tritium ions hopping from a Li_6 to its nearest neighbour O_6 layer. The final class, C3, involves processes where the tritium crosses the mixed cation layer and consequently have larger jump distances.

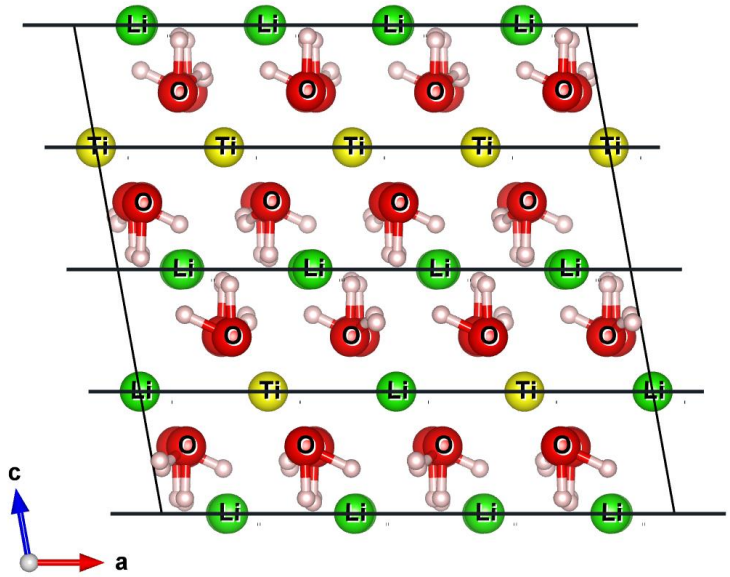

Figure 5: 2×1×1 supercell of Li_2TiO_3 illustrating the location of the tritium interstitial sites.

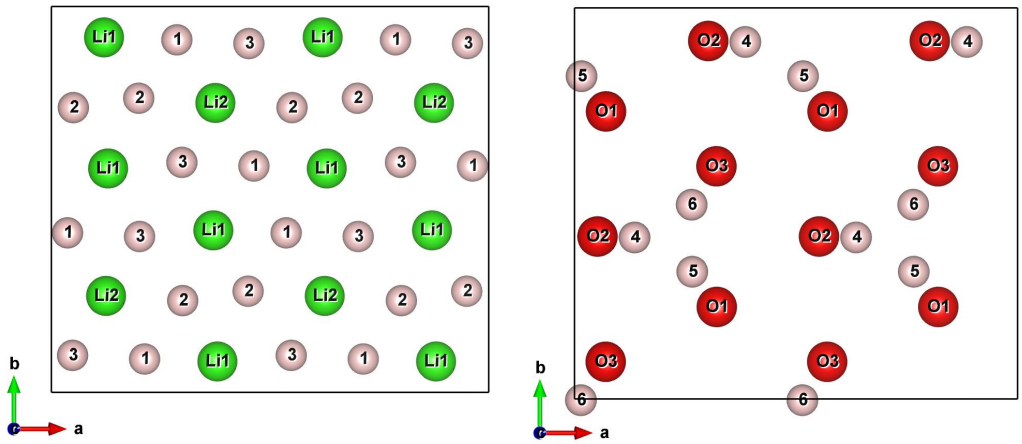

(a) (b)

Figure 6: Tritium sites near the (a) Li_6 and (b) O_6 layers

Table 4: Calculated diffusion path distances, d, and energy barriers for tritium hops between different interstitial sites in a Li_2TiO_3 crystal for different classes of independent local minimum energy paths as defined in Shi *et al.*[9]

Diffusion Class	Pathway	d (Å)		Barrier (eV)	
		Present work	Shi *et al.*[9]	Present work	Shi *et al.*[9]
C1 [Li_6-Li_6]	1↔1	1.77	1.68	0.49	0.33
	2↔2	1.77	1.69	0.51	0.33
	3↔3	1.98	2.04	0.73	0.55
	1→2 (1←2)	1.68	1.58	0.46 (0.45)	0.29 (0.29)
	2→3 (2←3)	1.82	1.73	0.60 (0.45)	0.47 (0.30)
	1→3 (1←3)	1.86	1.80	0.62 (0.46)	0.48 (0.31)
C2 [Li_6-O_6]	1→4 (1←4)	1.08	1.15	0.09 (0.01)	0.10 (0.00)
	2→5 (2←5)	1.08	1.15	0.08 (0.02)	0.09 (0.00)
	3→6 (3←6)	1.31	1.41	0.11 (0.16)	0.11 (0.11)
C3 [O_6-Li_2Ti_4-O_6]	6↔6	2.81	2.77	1.07	0.97
	5↔5	3.11	3.08	1.05	1.00
	4→5 (4←5)	3.15	3.12	0.98 (0.98)	0.91 (0.92)
	4→6 (4←6)	2.99	2.96	1.00 (0.96)	0.93 (0.86)

Analysis of the data presented in Table 4 shows that while the activation energies predicted here are mostly higher than those of Shi *et al.* the overall picture remains the same. The processes with the lowest activation energies are the rotations around the oxygen ions of the C2 class, where the barriers can be as low as 0.01 eV. In fact, these barriers are so low that Shi *et al.* could not calculate a barrier for the reorientations around the O1 and O2 ions.[9] It is important to note that there must be a barrier as otherwise the interstitial site itself would not be stable. Shi *et al.* deduced that tritium sites 4 and 5 were actually not energy minimums, but cusps along a very flat potential energy surface. For diffusion around the pure lithium layer (C1 class) the barriers calculated here are 0.15 eV higher in energy than Shi *et al.*, however, the ordering is identical with the diffusion from the tritium interstitial site $1 \rightarrow 2$ having the lowest energy barrier of 0.45 eV. This process is incapable of facilitating bulk diffusion of tritium on its own. The lowest energy pathway to net tritium diffusion in the *xy*-plane can be achieved through a combination of $1 \rightarrow 2$, $2 \rightarrow 2$, $2 \rightarrow 1$ and $1 \rightarrow 1$ processes with an overall activation energy of 0.51 eV. The energy barriers for the hops across the mixed cation layer have the longest jump distances and, as a consequence,

the highest barriers. Table 4 shows that migration from interstitial site 6 $\rightarrow$ 4 is the lowest energy process that traverses the mixed cation layer in agreement with Shi *et al.*[9] This is also the overall barrier to interstitial tritium diffusion in the z-direction. Overall, therefore, the results presented in Table 4 support the prediction of highly anisotropic tritium diffusion as an interstitial.

Tritium Diffusion in the Vicinity of Lithium Vacancies

As the burn-up of lithium increases the concentration of lithium vacancy defects in the ceramic pebbles is anticipated to increase. The lithium vacancy defect is negatively charged and the tritium interstitials are positively charged therefore the two defects will become bound due to the Coulomb attraction between them. However, despite being bound to the vacancy defect the tritium ions remain bonded to the oxygen ions as hydroxyls, with slightly increased bond lengths. Due to its distorted rocksalt structure, all lithium ions in Li_2TiO_3 are octahedrally co-ordinated with six oxygen ions surrounding them, each of which could form a bond with tritium. As illustrated in Figure 3 the lithium ions in the pure lithium layers have a very similar arrangement of nearest neighbour cations, however, the lithium in the mixed cation layer has a different local environment. This difference in the nearest neighbour cations leads to significant differences in the behaviour of tritium in the region surrounding the vacancy as will be described below.

Figure 7 shows the positions of the tritium interstitial sites surrounding the Li3 site and how these positions change when the lithium ion is removed. The image shows that the positions of the tritium sites that are aligned close to the z-axis are relatively unperturbed by the vacancy, however, the hydroxyl groups that lie closest to the xy-plane become reorientated such that they point towards the now vacant site. For simplicity it is assumed that as the position of the hydroxyl groups aligned along z are unperturbed the energy barrier to diffuse from this site away from the vacancy can be considered to be the interstitial activation energy as discussed above. A number of barriers for tritium migration to form hydroxyls on

the second nearest neighbour oxygen sites were considered, however, as their energies are significantly higher these processes are not discussed further.

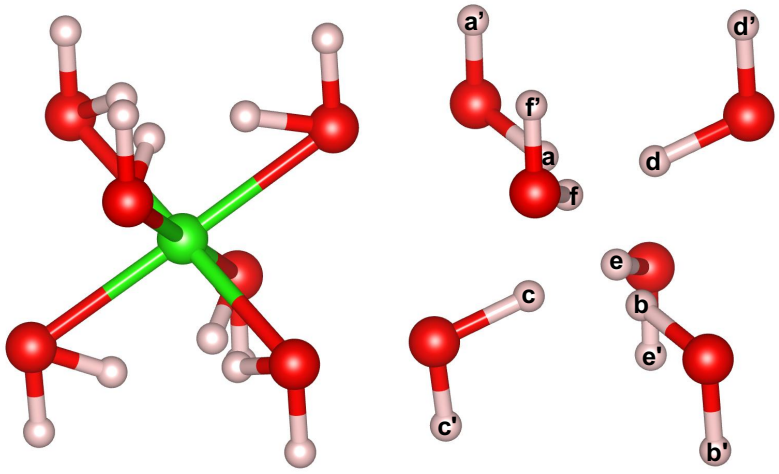

(a) (b)

Figure 7: Tritium interstitial site modifications for a Li3 vacancy in the mixed cation layer. The green and red spheres represent the lithium and oxygen ions while the white spheres represent the possible tritium interstitial sites. (a) Each of the six oxygen ions bonded to a lithium ion has two possible tritium interstitial sites. (b) On removing the lithium ion, six of these sites (a' - f') pointing away from the vacancy remain unaffected while the other six sites (a - f) now point towards the vacancy.

Therefore, it is only necessary to calculate the energy barriers for the reorientation which can be combined with the interstitial barriers calculated above. Migration barriers to diffusion within the vacancy itself will be considered later. The energy barriers for the reorientation, diffusion away from the reorientated site and the overall escape are presented in Table 5. Table 5 shows that, for a vacancy on the Li3 site, there are four reorientations that have an energy barrier in the range 0.54-0.56 eV and the two remaining pathways have higher energies at 0.74 eV. As evident from the significantly migration energies for the reverse process, the formation energy of the complex with the hydroxyl pointing away from the vacancy is higher than when the hydroxyl points directly towards the formerly occupied lattice site.

Once the reorientations have taken place the tritium ions can diffuse as if they were members of the interstitial C1 class. This is because the de-trapped sites for the Li3 vacancy remained unaffected due to the presence of the vacancy and are thus equivalent to the

Table 5: Calculated diffusion path distances, d and energy barriers for trapping and detrapping of a tritium inside a Li3 vacancy.

Pathway	d (Å)	Barrier (eV)			Escape Pathway
		Forward	Reverse	Escape	
a→a'	1.78	0.55	0.01	1.06	a'(1) →2→2→1→1
b→b'	1.79	0.54	0.01	1.05	b'(1) →2→2→1→1
c→c'	1.80	0.56	0.005	1.065	c'(2) →2→1→1→2
d→d'	1.89	0.74	0.09	1.38	d'(3) →3→1→2→3
e→e'	1.90	0.74	0.10	1.37	e'(3) →3→1→2→3
f→f'	1.78	0.56	0.01	1.06	f'(2) →2→1→1→2

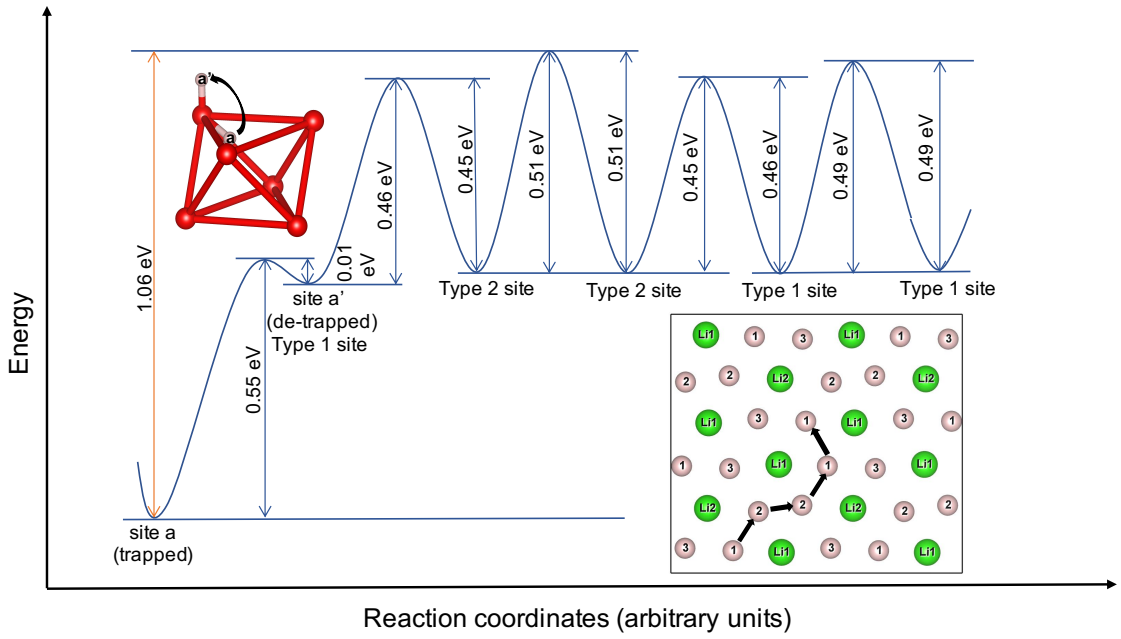

Figure 8: Energy barriers corresponding to the escape route for a tritium trapped in a Li3 vacancy for the pathway a→a'(1) →2→2→1→1 with a total escape barrier of 1.06 eV.

interstitial tritium sites of types 1, 2 and 3 as shown in Figure 6(a). These barriers are then combined with the re-orientation energy to give the overall barriers for escape from the Li3 vacancy for each individual pathway. Figure 8 shows the a→a' pathway where the overall barrier for escape was calculated as 1.06 eV. The escape barriers are in the range of 1.05-1.38 eV as tabulated in Table 5.

For the Li1 and Li2 vacancies the situation is more complicated. The tritium positions surrounding an occupied and vacant Li1 site are shown in Figure 9. As was the case for the Li3 site, there are six nearest neighbours surrounding the Li site. If the Li site is occupied there are two possible hydroxyl arrangements on each oxygen. Similar to what was observed for the Li3 site, the hydroxyl positions closest to the xy-plane reorientate to point towards the vacancy defect. However, whereas in the Li3 case the remaining hydroxyls were relatively unaffected, for the Li1 and Li2 sites four of these positions no longer form stable defect sites, while the remaining two stayed very close to their initial positions. The reason for the different behaviour is the presence of the Ti in the mixed cation layer being on average closer to the unstable hydroxyl sites. Therefore, in addition to determining the barriers for the reorientation, the barriers to jumps to the second nearest neighbour sites evident in Figure 9 are also considered.

Irrespective of the pathway taken to escape from positions directly adjacent to the vacancy, the tritium will end up in de-trapped positions equivalent to interstitial sites 4 or 5. The migration barriers for tritium diffusion away from these interstitial sites is through a combination of C1 and C2 classes (see Table 4) ensuring that the effective barrier for escape is in the range of 1.1-1.34 eV as tabulated in Table 6. This range of energy barriers is similar to the ones obtained for the Li3 vacancy. These results suggest that the introduction of Li vacancies into either the pure lithium or mixed cation layers could have a significant impact on overall tritium diffusion if the vacancy defects are considered to be immobile.

Table 7 shows the energy barriers for diffusion between the hydroxyl groups pointed towards the lithium vacancy defects compared to the previous results of Li *et al.*[10] The

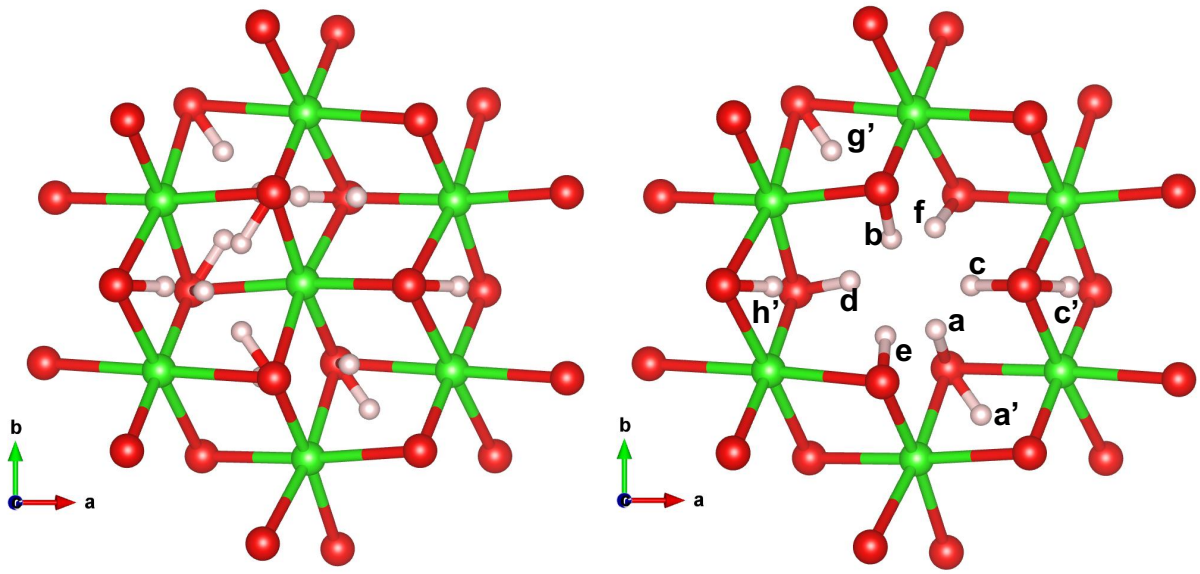

(a) (b)

Figure 9: Tritium interstitial site modifications for a Li1 vacancy. (a) Similar to the Li3 case, each of the six oxygen ions bonded to the lithium ion has two possible interstitial sites that can accommodate the tritium. However, here only two of these sites point away from the Li ion (a' and c'), while two second neighbour sites (g' and h') lie in close proximity to the ion. (b) On removing the Li1 ion, ten out of twelve sites collapse to the six sites pointing towards the vacancy, while the other two sites (a' and c') remain unaffected. Tritium trapped at sites a and c can reorient to a' and c' respectively similar to the Li3 vacancy, while tritium trapped at other sites can escape via the g' and h' sites whichever is nearer. The entire process is similar in the case of a Li2 vacancy.

Table 6: Calculated diffusion path distances, d and energy barriers for trapping and detrapping of a tritium inside a Li1 vacancy.

Pathway	d (Å)	Barrier (eV)			Escape Pathway
		Forward	Reverse	Escape	
a→a'	1.66	0.66	0.00	1.10	a'(4)→1 →2→2→1→1→4
b→g'	2.22	1.25	0.63	1.25	g'(4)→1 →2→2→1→1→4
b→h'	2.27	1.34	0.75	1.34	h'(5)→2 →2→1→1→2→5
c→c'	1.74	0.69	0.00	1.14	c'(5)→2 →2→1→1→2→5
d→g'	2.28	1.25	0.63	1.25	g'(4)→1 →2→2→1→1→4
d→h'	2.24	1.19	0.60	1.19	h'(5)→2 →2→1→1→2→5
e→h'	2.19	1.28	0.67	1.28	h'(5)→2 →2→1→1→2→5
f→g'	2.21	1.26	0.63	1.26	g'(4)→1 →2→2→1→1→4

results in Table 7 shows that the activation energies for tritium to move around the vacant site range from 0.66 eV to 1.0 eV. Hops between sites that involve traversing the vacant lithium site have larger jump distances and are predicted by Li *et al.* to have significantly higher barriers. The results presented here also predict very high barriers to traversing the vacant Li site, however, much lower barriers are predicted to traverse the Li1 and Li2 vacancies. The reason for this is that the LST/QST methodology is detecting mechanisms that make the tritium diffuse via an intermediate state that is bonded to one of the other neighbouring oxygen ions. This does not affect the overall observation that tritium will preferentially diffuse around the periphery of the vacancy rather than crossing the vacant site.

In general the predicted energies for tritium migration around the lithium vacancy are higher than those calculated by Li *et al.* Although it is noted that performing a direct comparison to these previous results is complicated due to difficulties identifying the corresponding pathways. There are, however, methodological differences that may account for this difference. In their calculations, Li *et al.* allowed the simulation supercell to relax when performing the geometry optimisation of the initial and final structures, while in the simulations presented here these were fixed to those determined for the perfect cell. The calculation of volume changes for charged supercells is poorly defined leading to unrealistic volume changes.[32] While the simulations of Li *et al.* were all charge neutral, that is not the case here, therefore, to ensure consistency between the results the simulation supercells remain fixed throughout.

Diffusion of the $\{\mathrm{T}_i^{1+} : V_{\mathrm{Li}}^{1-}\}^0$ Cluster

The two previous sections have examined how tritium can move as an interstitial and how it diffuses in the vicinity of a lithium vacancy. In these simulations it is only the movement of the tritium itself that is considered and the remaining ions in the system are effectively spectators in the process. In this final section, processes where the presence of the lithium

vacancy may help to promote tritium diffusion are examined. An example of how this process may occur is presented in Figure 10, which shows a process whereby the lithium vacancy with a hydroxyl group bound to it moves to an adjacent lattice site. As clearly indicated in the diagram the lithium ion moves to the right while the tritium ions moves to the left. If this is combined with the diffusion around the vacancy, as discussed above, then it is possible to create a collaborative mechanism that enables macroscopic tritium diffusion without detrapping of the tritium from the Li vacancy.

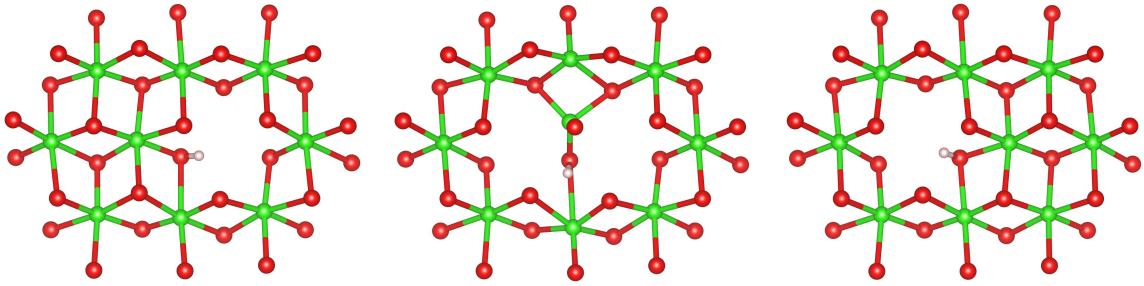

(a) (b) (c)

Figure 10: An example of the collaborative diffusion mechanism of the $\{\mathrm{T}_i^{1+} : V_{\mathrm{Li}}^{1-}\}^0$ cluster. In this case the system evolves from an initial lattice configuration (a) where a lithium on an Li1 site moves onto a neighbouring Li1 vacancy containing a tritium, via transition state (b) to a final state (c) with the simultaneous diffusion of tritium in the opposite direction

The energy barriers for the migration of the different lithium vacancy defects in the $\{\mathrm{T}_i^{1+} : V_{\mathrm{Li}}^{1-}\}^0$ cluster are presented in Table 8. From the table it is possible to see that the lowest energy barrier is for the $\mathrm{V}_{\mathrm{Li1}}^{-1} \rightarrow \mathrm{V}_{\mathrm{Li2}}^{-1}$ process with an energy of 0.98 eV for the forward jump and 1.00 eV for the reverse jump. Other barriers are larger with the highest being for the $\mathrm{V}_{\mathrm{Li3}}^{-1} \rightarrow \mathrm{V}_{\mathrm{Li1}}^{-1}$ process. Combining the $\mathrm{V}_{\mathrm{Li1}}^{-1} \rightarrow \mathrm{V}_{\mathrm{Li2}}^{-1}$ process with diffusion barriers for tritium to move around within the Li1 and Li2 vacancies as shown in Table 7, where, with the exception of the diagonal jumps within the octahedron, the barriers are always smaller than 1 eV, gives an overall energy barrier to diffusion of $\approx$ 1 eV. This barrier is smaller than the barriers predicted in Tables 5 and 6 for the overall tritium escape from the lithium vacancy sites and to diffuse as an interstitial. This implies that if a tritium ion does become bound to a Li1 or Li2 vacancy in the β-$\mathrm{Li_2TiO_3}$ crystal, the two will diffuse some distance

together before the tritium eventually detraps.

Conclusion

Energy barriers for the migration of lithium vacancy defects, tritium and their clusters in β-Li_2TiO_3 have been determined using DFT. From the data presented above the following conclusions can be drawn:

- There is a small anisotropy in the energy barriers for diffusion of the lithium vacancy defect. For diffusion in the z-direction the lithium vacancy can undergo a series of Li2→Li3 and Li3→Li2 transitions resulting in an overall barrier of 0.47 eV. This compares with diffusion in the xy-plane, where the minimum barrier is 0.50 eV for Li1→Li1 process.

- For tritium as an interstitial the activation energy for diffusion in the xy-plane has an overall energy barrier of 0.52 eV. Diffusion in the z-direction would require the tritium to traverse the mixed cation layer. The barriers to cross this layer are predicted to be greater than 0.98 eV, therefore, the diffusivity of tritium interstitials in the xy-plane is expected to be much greater than along z.

- The barriers for a tritium ion to escape from a T^0_{Li} cluster on the Li1 and Li2 sites is in the range of 1.1 - 1.34 eV and that for the Li3 site it is between 1.05 - 1.38 eV.

- The minimum energy barrier for the co-operative mechanism whereby the V^{-1}_{Li} and T_i^{1+} defects move through the lattice without the tritium de-trapping is found to be ≈1 eV for the $V^{-1}_{Li1} \rightarrow V^{-1}_{Li2}$ process. This is smaller than that calculated for escape from the lithium vacancy sites. Ultimately, this suggests that if a tritium ion becomes bound to a Li1 or Li2 vacancy, the pair will travel through the lattice together.

- Once bound to a lithium vacancy the energy barrier to further diffusion of the tritium, whether via de-trapping from the vacancy or diffusing as a cluster, is $\geq$ 1 eV. This is

significantly greater than the activation energy for the tritium interstitial (0.47 eV). As the concentration of lithium vacancies is anticipated to increase as the lithium burn-up is increased this implies that tritium will become more difficult to extract, leading to increased tritium retention later in the pebbles' lifetime.

Acknowledgement

The authors acknowledge funding from EPSRC under contract number EP/R006288/1. Computational resources were provided via our membership of the UK's HEC Materials Chemistry Consortium, which is funded by EPSRC (EP/L000202, EP/R029431), this work used the ARCHER UK National Supercomputing Service (http://www.archer.ac.uk).

References

(1) Raffray, A. R.; Akiba, M.; Chuyanov, V.; Giancarli, L.; Malang, S. Breeding blanket concepts for fusion and materials requirements. *J. Nucl. Mater.* **2002**, *307-311*, 21–30.

(2) Zheng, S.; Todd, T. N. Study of impacts on tritium breeding ratio of a fusion DEMO reactor. *Fus. Eng. Des.* **2015**, *98-99*, 1915–1918.

(3) Tsuchiya, A.; Yamauchi, Y.; Nobuta, Y.; Hino, T.; Akiba, M.; Enoeda, M. Influence of surface condition on deuterium release from Li_2TiO_3 pebble. *Fus. Eng. Des.* **2014**, *89*, 1280–1283.

(4) Kulsartov, T.; Tazhibayeva, I.; Gordienko, Y.; Chikhray, E.; Tsuchiya, K.; Kawamura, H.; Kulsartov, A. Study of tritium and helium release from irradiated lithium ceramic Li_2TiO_3. *Fus. Eng. Des.* **2011**, *60*, 1139–1142.

(5) Kinjyo, T.; Nishikawa, M.; Enoeda, M.; Fukada, S. Tritium diffusivity in crystal grain

of Li_2TiO_3 and tritium release behavior under several purge gas conditions. *Fus. Eng. Des.* **2008**, *83*, 580–587.

(6) Tanifuji, T.; Yamaki, D.; Nasu, S.; Noda, K. Tritium release behavior from neutron-irradiated Li_2TiO_3 single crystal. *J. Nucl. Mater.* **1998**, *258-263*, 543–548.

(7) Zhu, D.; Oda, T.; Shono, Y.; Tanaka, S. Release behavior of hydrogen isotopes thermally sorbed in Li_2TiO_3 single crystal. *J. Nucl. Mater.* **2013**, *442*, S437–S441.

(8) Murphy, S. T. Tritium solubility in Li_2TiO_3 from first-principles simulations. *J. Phys. Chem. C* **2014**, *118*, 29525–29532.

(9) Shi, Y.; Qi, J.; Han, Y.; Lu, T. Anisotropic diffusion of a charged tritium interstitial in Li_2TiO_3 from first-principles calculations. *Phys. Rev. Appl.* **2018**, *10*, 024021.

(10) Li, K.; Yang, W.; Wang, W.-H.; Li, Y.-T. First principles study of tritium diffusion in Li_2TiO_3 crystal with lithium vacancy. *Materials* **2018**, *11*, 2383.

(11) Izquierdo, G.; West, A. R. Phase equilibria in the system Li_2O-TiO_2. *Mater. Res. Bull.* **1980**, *15*, 1655–1660.

(12) Kleykamp, H. Phase equilibria in the Li–Ti–O system and physical properties of Li_2TiO_3. *Fus. Eng. Des.* **2002**, *61-62*, 361–366.

(13) Lang, G. Die Kristallstruktur einiger Vertreter der Verbindungsklasse $Me_2(I)Me(IV)O_3$ als Beitrag zur Aufklurung der Ordnungsphase von Li_2TiO_3. *Z. Anorg. Allg. Chem.* **1954**, *276*, 77–94.

(14) Kataoka, K.; Takahashi, Y.; Kijima, N.; Nagai, H.; Akimoto, J.; Idemoto, Y.; ichi Ohshima, K. Crystal growth and structure refinement of monoclinic Li_2TiO_3. *Mater. Res. Bull.* **2009**, *44*, 168–172.

(15) Tarakina, N. V.; Neder, R. B.; Denisova, T. A.; Maksimova, L. G.; Baklanova, Y. V.; Tyutyunnik, A. P.; Zubkov, V. G. Defect crystal structure of new $TiO(OH)_2$ hydroxide and related lithium salt Li_2TiO_3. *Dalton Trans.* **2010**, *39*, 8168–8176.

(16) Murphy, S. T.; Hine, N. D. Point defects and non-stoichiometry in Li_2TiO_3. *Chem. Mater.* **2014**, *26*, 1629–1638.

(17) Hohenberg, P.; Kohn, W. Inhomogeneous electron gas. *Phys. Rev.* **1964**, *136*, B864–B871.

(18) Kohn, W.; Sham, L. J. Self-consistent equations including exchange and correlation effects. *Phys. Rev.* **1965**, *140*, A1133–A1138.

(19) Payne, M. C.; Teter, M. P.; Allan, D. C.; Arias, T.; Joannopoulos, a. J. Iterative minimization techniques for *ab initio* total-energy calculations: molecular dynamics and conjugate gradients. *Rev. Mod. Phys.* **1992**, *64*, 1045.

(20) Clark, S. J.; Segall, M. D.; Pickard, C. J.; Hasnip, P. J.; Probert, M. I.; Refson, K.; Payne, M. C. First principles methods using CASTEP. *Z. Kristallogr.* **2005**, *220*, 567–570.

(21) Perdew, J. P.; Burke, K.; Ernzerhof, M. Generalized gradient approximation made simple. *Phys. Rev. Lett.* **1996**, *77*, 3865.

(22) Murphy, S. T.; Hine, N. D. M. Anisotropic charge screening and supercell size convergence of defect formation energies. *Phys. Rev. B* **2013**, *87*, 094111.

(23) Monkhorst, H. J.; Pack, J. D. Special points for Brillouin-zone integrations. *Phys. Rev. B* **1976**, *13*, 5188–5192.

(24) Methfessel, M.; Paxton, A. T. High-precision sampling for Brillouin-zone integration in metals. *Phys. Rev. B* **1989**, *40*, 3616–3621.

(25) Govind, N.; Petersen, M.; Fitzgerald, G.; King-Smith, D.; Andzelm, J. A generalized synchronous transit method for transition state location. *Comp. Mater. Sci.* **2003**, *28*, 250–258.

(26) Kuganathan, N.; Kordatos, A.; Fitzpatrick, M.; Vovk, R.; Chroneos, A. Defect process and lithium diffusion in Li_2TiO_3. *Solid State Ionics* **2018**, *327*, 93–98.

(27) Ruprecht, B.; Wilkening, M.; Uecker, R.; Heitjans, P. Extremely slow Li ion dynamics in monoclinic Li_2TiO_3–probing macroscopic jump diffusion via ^{7}Li NMR stimulated echoes. *Phys. Chem. Chem. Phys.* **2012**, *14*, 11974–11980.

(28) Monchak, M.; Dolotko, O.; Muhlbauer, M. J.; Baran, V.; Senyshyn, A.; Ehrenberg, H. Monoclinic β-Li_2TiO_3: Neutron diffraction study and estimation of Li diffusion pathways. *Solid State Sci.* **2016**, *61*, 161–166.

(29) Mukai, K.; Yashima, M.; Hibino, K.; Terai, T. Experimental visualization of interstitialcy diffusion of Li Ion in β-Li_2TiO_3. *ACS Appl. Energy Mater.* **2019**, *2*, 5481–5489.

(30) Islam, M. M.; Bredow, T. Lithium diffusion pathways in β-Li_2TiO_3: a theoretical study. *J. Phys. Chem. C* **2016**, *120*, 7061–7066.

(31) Vijayakumar, M.; Kerisit, S.; Yang, Z.; Graff, G. L.; Liu, J.; Sears, J. A.; Burton, S. D.; Rosso, K. M.; Hu, J. Combined 6, 7Li NMR and molecular dynamics study of Li diffusion in Li_2TiO_3. *J. Phys. Chem. C* **2009**, *113*, 20108–20116.

(32) Goyal, A.; Mathew, K.; Hennig, R. G.; Chernatynskiy, A.; Stanek, C. R.; Murphy, S. T.; Andersson, D. A.; Phillpot, S. R.; Uberuaga, B. P. The Conundrum of Relaxation Volumes in First-Principles Calculations of Charged Defects in UO_2. *App. Sci.* **2019**, *9*, 5276.

Table 7: Calculated diffusion path distances, d, and energy barriers for 15 possible types of tritium hops around the vacant lithium sites corresponding to Li1, Li2 and Li3 vacancies in a Li2TiO3 crystal. The first 12 of these paths are tritium hops around the periphery of the Li vacancy while for the last 3 paths, tritium has to traverse through the vacant lithium site.

	Pathway	Li1			Li2			Li3		
		d (Å)	Barrier (eV)		d (Å)	Barrier (eV)		d (Å)	Barrier (eV)	
			Forward	Reverse		Forward	Reverse		Forward	Reverse
Present work	a→c	1.27	0.66	0.66	1.55	0.66	0.68	1.59	0.89	0.89
	a→d	1.59	0.98	0.83	1.74	0.93	0.94	1.34	0.81	0.83
	a→e	1.45	0.78	0.66	1.33	0.75	0.86	1.63	0.91	0.93
	a→f	1.70	1.00	0.87	1.67	0.85	0.96	1.34	0.81	0.82
	b→c	1.58	0.82	0.97	1.73	0.92	0.94	1.34	0.81	0.82
	b→d	1.37	0.91	0.91	1.53	0.67	0.69	1.62	0.91	0.93
	b→e	1.62	0.85	0.87	1.64	0.84	0.96	1.35	0.81	0.83
	b→f	1.45	0.79	0.80	1.33	0.73	0.84	1.60	0.88	0.90
	c→e	1.71	1.00	0.87	1.69	0.84	0.94	1.35	0.90	0.91
	c→f	1.44	0.81	0.67	1.34	0.77	0.86	1.61	0.89	0.90
	d→e	1.43	0.80	0.82	1.34	0.77	0.87	1.66	0.96	0.96
	d→f	1.64	0.96	0.98	1.66	0.85	0.95	1.35	0.91	0.90
	a→b	2.06	1.02	0.88	2.30	0.90	0.89	2.08	3.15	3.15
	c→d	2.07	1.03	0.88	2.34	0.90	0.90	2.11	3.17	3.18
	e→f	2.34	0.92	0.91	1.93	1.90	1.90	2.13	3.19	3.18
Li *et al.*[10]	a↔c	1.62	0.71					1.85	0.85	
	a↔d	1.93	0.96					1.41	0.64	
	a↔e	1.86	0.80					1.86	0.86	
	a↔f	1.39	0.63					1.44	0.75	
	b↔c	1.92	0.95					1.40	0.66	
	b↔d	1.34	0.45					1.84	0.83	
	b↔e	1.61	0.62					1.44	0.75	
	b↔f	1.99	0.97					1.83	0.82	
	c↔e	1.62	0.62					1.41	0.64	
	c↔f	1.85	0.74					1.84	0.83	
	d↔e	1.99	0.98					1.85	0.85	
	d↔f	1.63	0.61					1.40	0.63	
	a↔b	2.28	3.07					2.27	2.97	
	c↔d	2.29	3.11					2.25	2.97	
	e↔f	2.58	3.00					2.27	2.98	

Table 8: Calculated diffusion energy barriers for collaborative diffusion mechanisms with simultaneous jumps of Li vacancy and tritium. The alphabets in the brackets represent the exact tritium sites in the Li vacancy

Pathway	Barrier (eV)	
	Forward	Reverse
$V_{Li1}^{-1} \rightarrow V_{Li1}^{-1}$, $T(f)_{Li1}^{0} \rightarrow T(c)_{Li1}^{0}$	1.22	1.36
$V_{Li1}^{-1} \rightarrow V_{Li2}^{-1}$, $T(f)_{Li1}^{0} \rightarrow T(a)_{Li2}^{0}$	0.98	1.00
$V_{Li3}^{-1} \rightarrow V_{Li1}^{-1}$, $T(c)_{Li3}^{0} \rightarrow T(f)_{Li1}^{0}$	1.72	1.58
$V_{Li3}^{-1} \rightarrow V_{Li2}^{-1}$, $T(c)_{Li3}^{0} \rightarrow T(a)_{Li2}^{0}$	1.29	1.15

Graphical TOC Entry